FRACTAL-LIKE MULTIPLE JETS IN ELECTROSPINNING PROCESS

by

Yu-Ke WU[a,b] and Yong LIU[c,d*]

[a] Jiangxi Province Key Laboratory of Polymer Micro/Nano Manufacturing and Devices, East China University of Technology, Nanchang, China
[b] Jiangxi Province Engineering Research Center of New Energy Technology and Equipment, East China University of Technology, Nanchang, China
[c] National Joint Engineering Research Center of High Performance Fibers and Textile Composites, Tiangong University, Tianjin, China
[d] School of Textiles, Tiangong University, Tianjin, China

Original scientific paper
https://doi.org/10.2298/TSCI2004499W

The electrospinning process is greatly affected by the instability of Taylor cone, an instable point can eject a jet, and multiple instable points can produce multiple jets. A fractal-like multi-jet phenomenon was found in electrospinning process with auxiliary electrodes, and main factors affecting the spinning process were studied experimentally, which included solution viscosity, surface tension, and conductivity. The fractal-like multi-jet is feasible to control the fiber morphology and its output.

Key words: *electrospinning, nanofibers, auxiliary electrode, fractal multi-jet*

Introduction

The electrospun nanofibers are generally between tens and hundreds of nanometers in size, which have the characteristics of high specific surface area, good fiber continuity and high porosity [1, 2]. The small fiber has high surface area, which produce a high geometric potential (surface energy) [3-7], as a result many fascinating properties have been found, for example, the lotus-like wetting property. As a high-tech and high value-added fiber material, nanofibers are indispensable key materials in the fields of biomedicine, tissue engineering, new energy and others [1, 2]. Their good properties have aroused great interest in the study of nanotechnology, material science and thermal science as well. However, the output of traditional single-needle electrospinning technology is about 0.01-0.05 g/h, which greatly restricts its development and industrial applications. In order to solve the problem, much effort has been made, the focus was put on various needleless electrospinning technology [8-11], multi-nozzle electrospinning technology [12], bubble electrospinning [13, 14], and macromolecular electrospinning [15-17].

Recently auxiliary electrodes (AE) became a hot topic in nanotechnology [18, 19], which can be used to exactly control the fiber's orientation. In our previous publications [20, 21], an auxiliary-electrode electrospinning was successfully designed, which could produce multiple jets. In this paper we will elucidate the mechanism of producing multiple jets from an instable Taylor cone.

* Corresponding author, e-mail: liuyong@tjpu.edu.cn

Experimental section

Materials

Polyvinyl alcohol (PVA) with an average molecular weight of 84000-89000 g/mol (Taiwan Changchun Oil Chemical Co. Ltd.) was purchased. Deionized water was used as the solvent, and all materials were used without further purification. The 8 wt.% PVA solution was prepared for experiment.

Apparatus

A traditional electrospinning (single needle) set-up is shown in fig. 1, which consisted of a 10 mL plastic syringe, a syringe pump (LSP02-1B, Baoding Longer Pump company, Baoding, China) and a needle spinneret (stainless steel hollow needle, with the outside diameter (OD) = 1.2 mm, the inner diameter (ID) = 0.79 mm), which was electrically connected to a positive polarity, high voltage power supply (DW-P803-4ACF2, Tianjin Dongwen Company, Tianjin, China), and a rectangle aluminum collector plate (30-40 cm in length and 0.02 cm thickness), which was connected to ground potential. The collector plate was located a working distance, h_0, from the needle tip, centered on and oriented orthogonally to the needle long axis. Polymer solution was supplied through the needle at a controlled feed rate using the syringe pump. Figure 2(a) shows a schematic representation of the multiple jets electrospinning experimental apparatus. A grounded stainless steel needle (ID = 0.5 mm) was used as the AE in this study, which was placed parallel to the spinneret. Figure 2(b) shows the enlarged image of electrospinning zone. The working distance, h_0, between the spinneret tip and the collector, was fixed at 15 cm. A solution feed rate was 2 mL/h, the distance between the electrode tip and the spinneret tip (ESD) was 2 cm. These parameters were fixed for all experiments, except where otherwise explicitly noted.

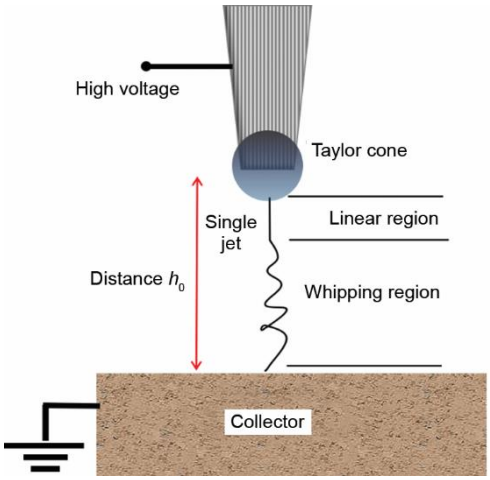

Figure 1. A traditional electrospinning apparatus

Result and discussion

Electrospinning and analysis

This paper focuses on a fractal-like electrospinning process. Liu *et al.* [22] first found the lightning-like jets in the bubble electrospinning. The fractal theory was successfully applied to controlling the shape of 2-D materials [23], and to designing optimally the spinneret [24], and now the fractal theory has become a useful mathematical tool to complex phenomena [25, 26]. Traditional electrostatic spinning device schematic diagram was shown in fig. 1. Its spinning process is as follows: a high voltage is applied at the end of the spinneret to make the surface of solution charged and deformed, and then a Taylor cone is formed at the end of the spinneret. When the applied voltage on the sprinkler exceeds a critical value, the charge repulsion force on the surface of the droplet overcomes the surface tension, and the jet

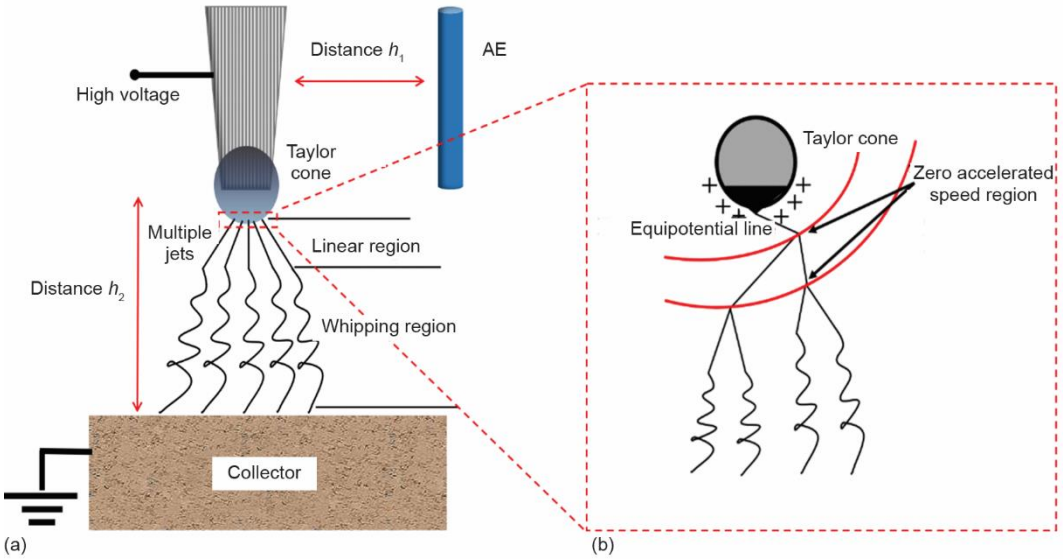

Figure 2. (a) Multiple jets electrospinning schematic with a grounded AE parallel to the spinneret, (b) enlarged image of electrospinning zone

is stretched by the electric field force in the high voltage electrostatic field. The molecule chains with enough entanglement are oriented along the axial direction of the jet and can balance the stretch of the electric field force. To maintain the continuity of the jet flow, nanofibers are solidified on the receiving plate as the solvent evaporates.

Figure 2(a) is a schematic diagram of the cusp AE electrospinning device. By applying the cusp AE into the spinning region and placing them parallel to the spinneret, multiple jets can be generated on a single spinneret. The spinning process is divided into two parts.

The first part is the region between the AE and the spinneret. When the distance between spinneret and AE (needle auxiliary distance) h_1 approaches 0, the electric field intensity near spinneret tends to be infinite, and the charged quantity of dielectrics tends to be infinite, leading to dielectrics being broken down and unable to spin. When h_1 approaches to an h_0 (see figs. 1 and 2), the area between the AE and spinneret is similar to another traditional electrospinning area. The AE becomes another receiving plate, and the jet flows toward the AE and the receiving plate. When h_1 approaches to infinity, the influence of AE on the spinning region is neglected. The spatial position of the AE has an important influence on the formation of multiple jets and the preparation of nanofibers.

Because the AE are grounded, the generated electrical potential is zero, and the potential of the receiving plate also generates complex equipotential lines in the zero-spinning region, as shown in fig. 2(b). After the jet is produced, it begins to accelerate to the receiving plate. When the high-speed jet moves along an equipotential line, the acceleration is zero, and the jet splits freely, forming splitting jets. At this time, any small disturbance will cause the instability of the vibration of the moving jet [27, 28], non-linear oscillation models can be solved by Taylor series method [29], the variational method [30-33], and He's frequency formulation [34, 35] to reveal the frequency-amplitude relation as discussed in [36-46]. In this paper, the region of jet bifurcation is called as the zero accelerated region. After the jet bifurcation, if the solvent does not evaporate completely, the jet continues to move along the direc-

tion of electric field force until the next equipotential line, the jet may be bifurcated again, which is beneficial to the further refinement of the fiber.

As shown in fig. 2(a), the spinning distance of traditional electrospinning is h_0, and the relationship between electric field strength E_0 and voltage V_0 can be approximately expressed:

$$E_0 = \frac{V_0}{h_0} \tag{1}$$

As shown in fig. 2, the distance between the AE and the spinneret is h_1, and the relationship between electric field strength E_1 and voltage V_1 can be approximately expressed:

$$E_1 = \frac{V_1}{h_1} \tag{2}$$

In electrospinning, when the applied voltage exceeds the critical voltage, the charge repulsion force overcomes the surface tension and the jet is generated from the surface of Taylor cone. When the electric field intensity of the two spinning devices is equal, from eqs. (1) and (2), it shows that:

$$\frac{V_0}{h_0} = \frac{V_1}{h_1} \tag{3}$$

Because the distance h_1 between AE and spinneret is much less than spinning distance, the critical voltage V_1 of jet generated by AE electrospinning is less than V_0, which can make it spin at lower voltage.

In order to explore the mechanism of fractal multi-jet produced by AE electrospinning and achieve the purpose of regulating the jet number. During the electrospinning process, the polymer solution was charged and deformed under high electric field. When the applied voltage reached the threshold value, a jet ejected from the Taylor cone. As shown in fig. 3(a), no jet formed when the applied voltage was lower than 5.12 kV for PVA-water solution. When the applied voltage was over such threshold voltage, the primary jet generally appeared first from the Taylor cone, followed by the jet fraction. As the voltage increased, 2 and 5 jets were produced 5.68 and 6.5 kV, figs. 3(b) and 3(c). Then, when the voltage increased at 10.21 and 11.05 kV, jet number reduced to 2 and 1. Bifurcation was found in different jet images. Such a phenomenon may be attributed to the different electric field distribution around the spinneret of electrospinning via AE.

Conclusion

The critical voltage of jet generated by electrospinning with cusp AE is less than that of traditional electrospinning, which is expected to be used in spinning experiments at lower voltage. The introduction of AE can produce complex equipotential lines in the spinning region. Jet with high initial velocity reaches the equipotential line in a short time, and when the acceleration tends to zero, the jet splits freely to form bifurcated jets. A mathematical model can be established to study the multiple jet system by the two-scale thermodynamics [47-49], when we watch the spinning process in a smaller spatiotemporal, a much precious hierarchical structure of the spinning jet can be detected.

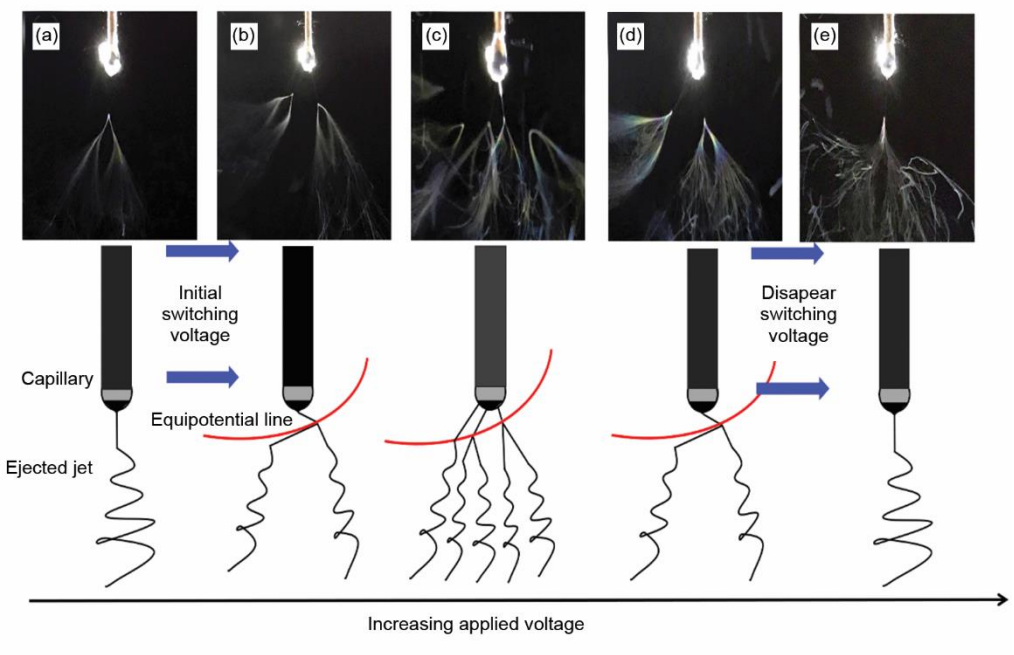

Figure 3. Schematic diagram of the formation of the Double-Switching Voltage; at relatively low applied voltage single jet is formed at the tip of the Taylor cone, as the applied voltage is increased the jet number increasing; increasing the applied voltage further results in decreasing of jet number

Acknowledgment

The authors gratefully acknowledge financial support by the National Natural Science Foundation of China (Grant No. 51573133) and Natural Science Foundation of Ningbo (No. 2018A610104).

Reference

[1] He, J. H., From Micro to Nano and from Science to Technology: Nano Age Makes the Impossible Possible, *Micro and Nanosystems, 12* (2020), 1, pp. 1-2
[2] He, J. H., *et al.* Review on Fiber Morphology Obtained by Bubble Electrospinning and Blown Bubble Spinning, *Thermal Science, 16* (2012), 5, pp. 1263-1279
[3] Tian, D., *et al.*, Geometrical Potential and Nanofiber Membrane's Highly Selective Adsorption Property, *Adsorption Science & Technology, 37* (2019), 5-6, pp. 367-388
[4] Fan, J., *et al.*, Explanation of the Cell Orientation in a Nanofiber Membrane by the Geometric Potential Theory, *Results in Physics, 15* (2019), Dec., ID 102537
[5] Li, X. X., *et al.*, Nanoscale Adhesion and Attachment Oscillation Under the Geometric Potential, Part 1: The Formation Mechanism of Nanofiber Membrane in the Electrospinning, *Results in Physics, 12* (2019), Mar., pp. 1405-1410
[6] Zhou, C. J., *et al.*, What Factors Affect Lotus Effect? *Thermal Science, 22* (2018), 4, pp. 1737-1743
[7] Yang, Z. P., *et al.*, On the Cross-Section of Shaped Fibers in the Dry Spinning Process: Physical Explanation by the Geometric Potential Theory, *Results in Physics, 14* (2019), Sept., ID 10234
[8] Liu, Z., *et al.*, Active Generation of Multiple Jets for Producing Nanofibres with High Quality and High Throughput, *Materials & Design, 94* (2016), Mar., pp. 496-501
[9] Liu, Z., *et al.*, Tunable Surface Morphology of Electrospun PMMA Fiber Using Binary Solvent, Applied *Surface Science, 364* (2016), Feb., pp. 516-521

[10] Liu, Z., *et al.*, Needle-Disk Electrospinning Inspired by Natural Point Discharge, *Journal of Materials Science, 52* (2017), 4, pp. 1823-1830
[11] Li, Z. J., *et al.* Preparation and Characterization of Long-Term Stable Pullulan Nanofibers Via in Situ Cross-Linking Electrospinning, *Adsorption Science & Technology, 37* (2019), 5-6, pp. 401-411
[12] Zhu, Z. M., *et al.*, A New Circular Spinneret System for Electrospinning – Numerical Approach and Electric Field Optimization, *Thermal Science, 23* (2019), 4, pp. 2229-2235
[13] Li, Y., He, J. H., Fabrication and Characterization of ZrO_2 Nanofibers by Critical Bubble Electrospinning for High-Temperature-Resistant Adsorption and Separation, *Adsorption Science & Technology, 37* (2019), 5-6, pp. 425-437
[14] Peng, N. B., *et al.*, A Rachford-Rice-Like Equation for Solvent Evaporation in the Bubble Electrospinning, *Thermal Science, 22* (2018), 4, pp. 1679-1683
[15] Tian, D., He, J. H. Macromolecular Electrospinning: Basic Concept & Preliminary Experiment, *Results in Physics, 11* (2018), Dec., pp. 740-742
[16] Tian, D., *et al.*, Macromolecule Orientation in Nanofibers, *Nanomaterials, 8* (2018), 11, ID 918
[17] Zhou, C. J., *et al.*, Silkworm-Based Silk Fibers by Electrospinning, *Results in Physics, 15* (2019), Dec., 102646
[18] Xu, G. J., *et al.*, Accurate Fabrication of Aligned Nanofibers Via a Double-Nozzle Near-Field Electrospinning, *Thermal Science, 23* (2019), 4, pp. 2143-2150
[19] Chen, R. X., *et al.*, Numerical Approach to Controlling a Moving Jet's Vibration in an Electrospinning System: An Auxiliary Electrode and Uniform Electric Field, *Journal of Low Frequency Noise, Vibration and Active Control, 38* (2019), 3-4, pp. 1687-1698
[20] Wu, Y. K., *et al.*, Improved Fiber Uniformity and Jet Number in Multi-spinneret Electrospinning via Auxiliary Electrode, *Fibers and Polymers, 20* (2019), 6, pp. 1172-1179
[21] Liu, Y., *et al.*, Multi-Jet Electrospinning Via Auxiliary Electrode, *Materials Letters, 141* (2015), pp. 153-156
[22] Liu, H. Y., *et al.*, Lightning-Like Charged Jet Cascade in Bubble Electrospinning with Ultrasonic Vibration, *Journal of Nano Research, 27* (2014), Mar., pp. 111-119
[23] Li, J. Z., *et al.* Fractal-Theory-Based Control of the Shape and Quality of CVD-Grown 2D Materials, *Advanced Materials, 31* (2019), 35, 1902431
[24] Yang, W. X., *et al.*, Optimal Spinneret Layout in Von Koch Curves of Fractal Theory Based Needleless Electrospinning Process, *AIP Adances, 6* (2016), 6, 065223
[25] Li, X. X., He, J. H., Along the Evolution Process: Kleibers' 3/4 Law Makes Way for Burbner's Surface Law, A Fractal Approach, *Fractals, 27* (2019), 2, 1950015
[26] Tian, D., *et al.*, Hall-Petch Effect and Inverse Hall-Petch Effect: A Fractal Unification, *Fractals, 26* (2018), 6, 1850083
[27] Zhao, J. H, *et al.*, Needle's Vibration in Needle-Disk Electrospinning Process: Theoretical Model and Experimental Verification, *Journal of Low Frequency Noise, Vibration and Active Control, 38* (2019), 3-4, pp. 1338-1344
[28] Zhang, L., *et al.*, Vibration of an Axially Moving Jet in a Dry Spinning Process, *Journal of Low Frequency Noise, Vibration and Active Control, 38* (2019), 3-4, pp. 1125-1131
[29] He, J. H., Ji, F. Y., Taylor Series Solution for Lane-Emden Equation, *Journal of Mathematical Chemistry, 57* (2019), 8, pp. 1932-1934
[30] Nawaz, Y., *et al.*, An Effective Modification of He's Variational Approach to a Non-linear Oscillator, *Journal of Low Frequency Noise, Vibration and Active Control, 38* (2019), 3-4, pp. 1013-1022
[31] He, J. H., A Modified Li-He's Variational Principle for Plasma, *International Journal of Numerical Methods for Heat and Fluid Flow*, On-line first, https://doi.org/10.1108/HFF-06-2019-0523, 2019
[32] He, J. H., Lagrange Crisis and Generalized Variational Principle for 3D unsteady flow, International *Journal of Numerical Methods for Heat and Fluid Flow*, On-line first, https://doi.org/10.1108/HFF-07-2019-0577, 2019
[33] He, J. H., Sun, C., A Variational Principle for a Thin Film Equation, *Journal of Mathematical Chemistry. 57* (2019), 9, pp. 2075-2081
[34] He, J. H., The Simplest Approach to Non-linear Oscillators, *Results in Physics, 15* (2019), Dec., ID 102546
[35] He, J. H., The Simpler, the Better: Analytical Methods for Non-linear Oscillators and Fractional Oscillators, *Journal of Low Frequency Noise, Vibration and Active Control, 38* (2019), 3-4, pp. 1252-1260

[36] Ren, Z. F., Wu, J. B., He's Frequency-Amplitude Formulation for Non-linear Oscillator with Damping, *Journal of Low Frequency Noise, Vibration and Active Control*, *38* (2019), 3-4, pp. 1045-1049
[37] Ren, Z. F., Hu, G. F., He's Frequency-Amplitude Formulation with Average Residuals for Non-linear Oscillators, *Journal of Low Frequency Noise, Vibration and Active Control*, *38* (2019), 3-4, pp. 1050-1059
[38] Ren, Z. F., Hu, G. F., Discussion on the Accuracies of He's Frequency-Amplitude Formulation and its Modification with Average Residuals, *Journal of Low Frequency Noise, Vibration and Active Control*, *38* (2019), 3-4, pp. 1713-1715
[39] Wang, Q. L., *et al.*, A Short Remark on Ren-Hu's Modification of He's Frequency-Amplitude Formulation and the Temperature Oscillation in a Polar Bear Hair, *Journal of Low Frequency Noise, Vibration and Active Control*, *38* (2019), 3-4, pp. 1374-1377
[40] Hu, G. F., Deng, S. X., Ren's Frequency-Amplitude Formulation for Non-linear Oscillators, *Journal of Low Frequency Noise, Vibration and Active Control*, *38* (2019), 3-4, pp. 1681-1686
[41] Tao, Z. L., *et al.* Approximate Frequency-Amplitude Relationship for a Singular Oscillator, *Journal of Low Frequency Noise, Vibration and Active Control*, *38* (2019), 3-4, pp. 1036-1040
[42] He, C. H., *et al.*, A Complement to Period/Frequency Estimation of a Non-linear Oscillator, *Journal of Low Frequency Noise, Vibration and Active Control*, *38* (2019), 3-4, pp. 992-995
[43] Tao, Z. L., *et al.*, Frequency and Solution of an Oscillator with a Damping, *Journal of Low Frequency Noise, Vibration and Active Control*, *38* (2019), 3-4, pp. 1699-1702
[44] Wang, Y., An, J. Y., Amplitude-Frequency Relationship to a Fractional Duffing Oscillator Arising in Microphysics and Tsunami Motion, *Journal of Low Frequency Noise, Vibration and Active Control*, *38* (2019), 3-4, pp. 1008-1012
[45] Ren, Z. F., *et al.*, He's Multiple Scales Method for Non-linear Vibrations, *Journal of Low Frequency Noise, Vibration and Active Control*, *38* (2019), 3-4, pp. 1708-1712
[46] Yu, D. N., *et al.*, Homotopy Perturbation Method with an Auxiliary Parameter for Non-linear Oscillators, *Journal of Low Frequency Noise, Vibration and Active Control*, *38* (2019), 3-4, pp. 1540-1554
[47] He, J. H., Ji, F. Y., Two-Scale Mathematics and Fractional Calculus for Thermodynamics, *Thermal Science*, *23* (2019), 4, pp. 2131-2133
[48] He, J. H., A Simple Approach to One-Dimensional Convection-Diffusion Equation and Its Fractional Modification for E Reaction Arising in Rotating Disk Electrodes, *Journal of Electroanalytical Chemistry*, *854* (2019), ID 113565
[49] Fan, J., *et al.*, Fractal Calculus for Analysis of Wool Fiber: Mathematical Insight of its Biomechanism, *Journal of Engineered Fibers and Fabrics*, On-line first, https://doi.org/10.1177/1558925019872200, 2019

Paper submitted: April 8, 2019
Paper revised: November 1, 2019
Paper accepted: November 1, 2019